Inorg. Chem. **2003**, *42*, 4610–4618

High-Frequency and -Field EPR Spectroscopy of Tris(2,4-pentanedionato)manganese(III): Investigation of Solid-State versus Solution Jahn–Teller Effects

J. Krzystek,[†] Gregory J. Yeagle,[‡] Ju-Hyun Park,[§] R. David Britt,[‡] Mark W. Meisel,[§] Louis-Claude Brunel,[†] and Joshua Telser*,[||]

Center for Interdisciplinary Magnetic Resonance, National High Magnetic Field Laboratory, Florida State University, Tallahassee, Florida 32310, Department of Chemistry, University of California—Davis, Davis, California 95616, Department of Physics and Center for Condensed Matter Sciences, University of Florida, Gainesville, Florida 32611-8440, and Chemistry Program, Roosevelt University, 430 S. Michigan Avenue, Chicago, Illinois 60605-1394

Received December 10, 2002

High-frequency and -field electron paramagnetic resonance (HFEPR) spectroscopy of a classical coordination complex, $Mn(acac)_3$ (Hacac = 2,4-pentanedione), has been performed on both solid powder and frozen solution (in CH_2Cl_2/toluene, 3:2 v/v) samples. Parallel mode detection X-band EPR spectra exhibiting resolved ^{55}Mn hyperfine coupling were additionally obtained for frozen solutions. Magnetic susceptibility and field-dependent magnetization measurements were also made on powder samples. Analysis of the entire EPR data set for the frozen solution allowed extraction of the relevant spin Hamiltonian parameters: $D = -4.52(2)$; $|E| = 0.25(2)$ cm^{-1}; $g_{iso} = 1.99(1)$. The somewhat lower quality solid-state HFEPR data and the magnetic measurements confirmed these parameters. These parameters are compared to those for other complexes of Mn(III) and to previous studies on $Mn(acac)_3$ using X-ray crystallography, solution electronic absorption spectroscopy, and powder magnetic susceptibility. Crystal structures have been reported for $Mn(acac)_3$ and show tetragonal distortion, as expected for this Jahn–Teller ion (Mn^{3+}, $3d^4$). However, in one case, the molecule exhibits axial compression and, in another, axial elongation. The current HFEPR studies clearly show the negative sign of D, which corresponds to an axial (tetragonal) elongation in frozen solution. The correspondence among solution and solid-state HFEPR data, solid-state magnetic measurements, and an HFEPR study by others on a related complex indicates that the form of $Mn(acac)_3$ studied here exhibits axial elongation in all cases. Such tetragonal elongation has been found for Mn^{3+} and Cr^{2+} complexes with homoleptic pseudooctahedral geometry as well as for Mn^{3+} in square pyramidal geometry. This taken together with the results obtained here for $Mn(acac)_3$ in frozen solution indicates that axial elongation could be considered the "natural" form of Jahn–Teller distortion for octahedral high-spin $3d^4$ ions. The previous electronic absorption data together with current HFEPR and magnetic data allow estimation of ligand-field parameters for $Mn(acac)_3$.

Introduction

HFEPR,[1] defined here as $\nu \geq 94$ GHz and $B_0 \leq 25$ T, has been very successful in recent years in spectroscopically detecting and characterizing a variety of integer-spin (non-Kramers) transition metal complexes. Such complexes had been traditionally dubbed "EPR-silent" due to their typically large zfs and lack of a doubly degenerate $M_S = \pm 1/2$ Kramers doublet.[2] These include such transition metal ions as Cr(II),[3] Fe(II),[4] Ni(II),[5−7] V(III),[8] and particularly

* To whom correspondence should be addressed. E-mail: jtelser@roosevelt.edu. Phone: +1 312 341 3687. Fax: +1 312 341 3680.
[†] Florida State University.
[‡] University of California—Davis.
[§] University of Florida.
[||] Roosevelt University.

(1) Abbreviations used in the text: acac, anion of 2,4-pentanedione; AOM, angular overlap model; EPR, electron paramagnetic resonance; FC, field cooled; hfc, hyperfine coupling; HFEPR, high-frequency and -field EPR; LMCT, ligand-to-metal charge transfer; ZFC, zero-field cooled; zfs, zero-field splitting.

(2) Abragam, A.; Bleaney, B. *Electron Paramagnetic Resonance of Transition Ions*; Dover Publications: New York, 1986.
(3) Telser, J.; Pardi, L. A.; Krzystek, J.; Brunel, L.-C. *Inorg. Chem.* **1998**, *37*, 5769−5775.

10.1021/ic020712l CCC: $25.00
Published on Web 06/27/2003

Mn(III).[9−16] The number of publications describing various Mn(III) complexes underscores the importance of high-spin ($3d^4$, $S = 2$) Mn(III) in its role as a building block in molecular magnets,[17−26] as a catalyst,[27,28] and in biochemical reaction cycles.[29−33]

The specific Mn^{3+} system under study here is tris(2,4-pentanedionato)manganese(III), $Mn(acac)_3$. This well-known coordination complex has not been studied before by HFEPR, although a closely related complex, $Mn(dbm)_3$ (Hdbm = 1,3-diphenyl-1,3-propanedione), has been previously investigated by HFEPR as a polycrystalline solid.[9] $Mn(acac)_3$ has been previously studied by X-band EPR employing both parallel and perpendicular (conventional) mode detection; however, no quantitative analysis of the spectra was presented.[34]

Diketonates, such the 2,4-pentanedionato (acetylacetonato) ligand, form complexes with most transition metal ions, and the resulting O_6 donor set is similar to that found in aqua complexes[35] and in oxide lattices, such as Mn^{3+} in rutile.[36] This group of complexes of the high-spin $3d^4$ Mn^{3+} ion with O_6 donors should be a classic case of a Jahn−Teller distorted system.[37,38] In particular, this effect should appear either as an axial elongation or compression of the complex. As discussed previously,[2,36] for such $3d^4$ systems, an axial elongation corresponds to an $^5A_1$ ground state ("hole" in the d_{z^2} orbital) and results in the zfs parameter $D < 0$, while an axial compression corresponds to a $^5B_1$ ground state ("hole" in $d_{x^2-y^2}$), resulting in $D > 0$.

For most Mn(III) complexes, not only in numerous (often porphyrinic) configurations of square pyramidal geometry[11,13,28,39−41] but also in octahedral complexes with O/N donors,[9,14,35,36] the sign of D is negative. Most importantly, in the tris(diketonato) complex studied by HFEPR, $Mn(dbm)_3$, for which the crystal structure clearly showed tetragonal elongation, with a noticeable rhombic distortion, D was unequivocally found to be negative.[9] Negative D values were also found for octahedral Cr^{2+} with O_6 donor sets.[3,42] Gregson et al., however, performed powder magnetic susceptibility studies on $Mn(acac)_3$,[43] and reported a positive D value for this complex.

The principal motivation to revisit $Mn(acac)_3$ is to account for this discrepancy in type of Jahn−Teller distortion by subjecting the complex to a comprehensive physical investigation. The primary experimental technique was HFEPR, performed on the complex both in frozen solution and in the solid state. These experiments were supported by X-band EPR using parallel mode detection, which has been successfully used to quantitatively study Mn(III) in various chemical environments.[28,31−33] In addition, optical absorption spectroscopy was employed on the complex in fluid solution to compare our results with the older electronic absorption data,[37,38] and most importantly, powder magnetic susceptibility and field dependent magnetization measurements were

(4) Knapp, M. J.; Krzystek, J.; Brunel, L.-C.; Hendrickson, D. N. *Inorg. Chem.* **2000**, *39*, 281−288.
(5) Pardi, L. A.; Hassan, A. K.; Hulsbergen, F. B.; Reedijk, J.; Spek, A. L.; Brunel, L.-C. *Inorg. Chem.* **2000**, *39*, 159−164.
(6) Collison, D.; Helliwell, M.; Jones, V. M.; Mabbs, F. E.; McInnes, A. J. L.; Riedi, P. C.; Smith, G. M.; Pritchard, R. G.; Cross, W. I. *J. Chem. Soc., Faraday Trans.* **1998**, *94*, 3019−3025.
(7) van Dam, P. J.; Klaassen, A. A. K.; Reijerse, E. J.; Hagen, W. R. *J. Magn. Reson.* **1998**, *130*, 140−144.
(8) Tregenna-Piggott, P. L. W.; Weihe, H.; Bendix, J.; Barra, A.-L.; Güdel, H.-U. *Inorg. Chem.* **1999**, *38*, 5928−5929.
(9) Barra, A.-L.; Gatteschi, D.; Sessoli, R.; Abbati, G. L.; Cornia, A.; Fabretti, A. C.; Uytterhoeven, M. G. *Angew. Chem., Intl. Ed. Engl.* **1997**, *36*, 2329−2331.
(10) Goldberg, D. P.; Telser, J.; Krzystek, J.; Montalban, A. G.; Brunel, L.-C.; Barrett, A. G. M.; Hoffman, B. M. *J. Am. Chem. Soc.* **1997**, *119*, 8722−8723.
(11) Krzystek, J.; Telser, J.; Pardi, L. A.; Goldberg, D. P.; Hoffman, B. M.; Brunel, L.-C. *Inorg. Chem.* **1999**, *38*, 6121−6129.
(12) Krzystek, J.; Telser, J.; Hoffman, B. M.; Brunel, L.-C.; Licoccia, S. *J. Am. Chem. Soc.* **2001**, *123*, 7890−7897.
(13) Bendix, J.; Gray, H. B.; Golubkhov, G.; Gross, Z. *J. Chem. Soc., Chem. Commun.* **2000**, 1957−1958.
(14) Limburg, J.; Vrettos, J. S.; Crabtree, R. H.; Brudvig, G. W.; de Paula, J. C.; Hassan, A.; Barra, A.-L.; Duboc-Toia, C.; Collomb, M.-N. *Inorg. Chem.* **2001**, *40*, 1698−1703.
(15) Mossin, S.; Weihe, H.; Barra, A.-L. *J. Am. Chem. Soc.* **2002**, *124*, 8764−8765.
(16) Mossin, S.; Stefan, M.; ter Heerdt, P.; Bouwen, A.; Goovaerts, E.; Weihe, H. *Appl. Magn. Reson.* **2002**, *21*, 586.
(17) Aromi, G.; Claude, J. P.; Knapp, M. J.; Huffman, J. C.; Hendrickson, D. N.; Christou, G. *J. Am. Chem. Soc.* **1998**, *120*, 2977−2978.
(18) Aromi, G.; Knapp, M. J.; Claude, J. P.; Huffman, J. C.; Hendrickson, D. N.; Christou, G. *J. Am. Chem. Soc.* **1999**, *121*, 5489−5499.
(19) Artus, P.; Boskovic, C.; Yoo, J.; Streib, W. E.; Brunel, L.-C.; Hendrickson, D. N.; Christou, G. *Inorg. Chem.* **2001**, *40*, 4199−4210.
(20) Yoo, J.; Yamaguchi, A.; Nakano, M.; Krzystek, J.; Streib, W. E.; Brunel, L.-C.; Ishimoto, H.; Christou, G.; Hendrickson, D. N. *Inorg. Chem.* **2001**, *40*, 4604−4616.
(21) Caneschi, A.; Gatteschi, D.; Sessoli, R.; Barra, A. L.; Brunel, L. C.; Guillot, M. *J. Am. Chem. Soc.* **1991**, *113*, 5873−5874.
(22) Barra, A. L.; Caneschi, A.; Gatteschi, D.; Sessoli, R. *J. Am. Chem. Soc.* **1995**, *117*, 8855−8856.
(23) Miller, J. S.; Vazquez, C.; Calabrese, J. C.; McLean, R. S.; Epstein, A. J. *Adv. Mater.* **1994**, *6*, 217−221.
(24) Miller, J. S.; Calabrese, J. C.; McLean, R. S.; Epstein, A. J. *Adv. Mater.* **1992**, *4*, 498−501.
(25) Miller, J. S.; Vazquez, C.; Jones, N. L.; McLean, R. S.; Epstein, A. J. *J. Mater. Chem.* **1995**, *5*, 707−711.
(26) Granroth, G. E.; Meisel, M. W.; Chaparala, M.; Jolicoeur, T.; Ward, B. H.; Talham, D. R. *Phys. Rev. Lett.* **1996**, *77*, 1616−1619.
(27) Sheldon, R. A., Ed.; *Metalloporphyrins in Catalytic Oxidations*; Marcel Dekker: New York, 1994.
(28) Campbell, K. A.; Lashley, M. R.; Wyatt, J. K.; Nantz, M. H.; Britt, R. D. *J. Am. Chem. Soc.* **2001**, *123*, 5710−5719.
(29) Fridovich, I. *Annu. Rev. Biochem.* **1995**, *64*, 97−112 and references therein.
(30) Faulkner, K. M.; Liochev, S. I.; Fridovich, I. *J. Biol. Chem.* **1994**, *269*, 23471−23476.
(31) Campbell, K. A.; Yikilmaz, E.; Grant, C. V.; Gregor, W.; Miller, A.-F.; Britt, R. D. *J. Am. Chem. Soc.* **1999**, *121*, 4714−4715.
(32) Campbell, K. A.; Force, D. A.; Nixon, P. J.; Dole, F.; Diner, B. A.; Britt, R. D. *J. Am. Chem. Soc.* **2000**, *122*, 3754−3761.
(33) Britt, R. D.; Peloquin, J. M.; Campbell, K. A. *Annu. Rev. Biophys. Biomol. Struct.* **2000**, *29*, 463−495.
(34) Dexheimer, S. L.; Gohdes, J. W.; Chan, M. K.; Hagen, K. S.; Armstrong, W. H.; Klein, M. P. *J. Am. Chem. Soc.* **1989**, *111*, 8923−8925.
(35) Basler, R.; Tregenna-Piggott, P. L. W.; Andres, H.; Dobe, C.; Güdel, H.-U.; Janssen, S.; McIntyre, G. J. *J. Am. Chem. Soc.* **2001**, *123*, 3377−3378.
(36) Gerritsen, H. J.; Sabisky, E. S. *Phys. Rev.* **1963**, *132*, 1507−1512.
(37) Fackler, J. P., Jr.; Davis, T. S.; Chawla, I. D. *Inorg. Chem.* **1965**, *4*, 130−132.
(38) Davis, T. S.; Fackler, J. P., Jr.; Weeks, M. J. *Inorg. Chem.* **1968**, *7*, 1994−2002.
(39) Krzystek, J.; Telser, J.; Knapp, M. J.; Hendrickson, D. N.; Aromi, G.; Christou, G.; Angerhofer, A.; Brunel, L.-C. *Appl. Magn. Reson.* **2001**, *23*, 571−585.
(40) Behere, D. V.; Mitra, S. *Inorg. Chem.* **1980**, *19*, 992−995. In this work a single-crystal susceptibility measurement was also performed, and the sign of D was determined to be negative.
(41) Kennedy, B. J.; Murray, K. S. *Inorg. Chem.* **1985**, *24*, 1557−1560.
(42) Ono, K.; Koide, S.; Sekiyama, H.; Abe, H. *Phys. Rev.* **1954**, *96*, 38−39.
(43) Gregson, A. K.; Doddrell, D. M.; Healy, P. C. *Inorg. Chem.* **1978**, *17*, 1216−1219.

performed to link the current magnetic resonance results with the previous magnetic data of Gregson et al.[43] The results allow an analysis of the solution electronic structure of Mn(acac)$_3$ with the goal of resolving the question of axial compression versus elongation in this interesting Jahn−Teller system.

This study is a continuation of our efforts to apply HFEPR to non-Kramers transition metal ion complexes in general.[3,4,11,12,39,44] A secondary aim of this work is thus to advance this spectroscopic technique, in particular to demonstrate the ability to perform HFEPR of integer-spin complexes in an organic solvent frozen solution, as was shown earlier in aqueous solution.[3] The comparison between X-band parallel mode detection EPR and HFEPR is also instructive.

Experimental Section

Materials. Mn(acac)$_3$ was purchased from both Aldrich and Strem and used as a solid "as is" for the HFEPR studies and the magnetic measurements. Alternatively, the compound was ground and embedded in *n*-eicosane (Aldrich, $C_{20}H_{42}$, mp 37 °C) or in a KBr pellet. For production of a low-temperature glass, the material was dissolved in dichloromethane and subsequently toluene was added to achieve a proportion of 3:2 CH_2Cl_2/toluene by volume (both from Aldrich, spectroscopy grade). Both solvents had been thoroughly purged with nitrogen to reduce dissolved oxygen concentration. The final concentration of Mn(acac)$_3$ for HFEPR studies was about 100 mM, and a typical sample volume was 250 μL, while the X-band studies were performed on 10−25 mM solutions. Electronic absorption spectra of Mn(acac)$_3$ in cyclohexane and in 3:2 CH_2Cl_2/toluene solutions at concentrations of 1 mM for the visible region (400−900 nm) and 10 mM for the NIR region (900−2000 nm) were recorded using a Jasco V-570 spectrophotometer.

EPR Instrumentation. A locally constructed HFEPR spectrometer was used, described previously.[45] It is a transmission-type device based on propagating the millimeter and submillimeter waves in cylindrical lightpipes and does not employ a resonator. Temperature control was achieved with an Oxford Instruments CF1200 continuous-flow liquid-helium cryostat and an ITC503 controller. The detector was a liquid-helium-cooled InSb bolometer from QMC Instruments. Magnetic field modulation was employed with the ensuing phase-sensitive detection using a lock-in amplifier.

X-band EPR spectra were recorded on a Bruker ECS106 system with a Bruker dual mode cavity capable of both parallel (TE012) and perpendicular (TE102) mode polarizations of the applied magnetic field. Temperature control was achieved with an Oxford Instruments ESR900 liquid-helium cryostat and an ITC503 controller.

Magnetic Measurements. The procedure used for recording and analyzing magnetic data was the same as in our previous study of pseudotetrahedral Ni(II) complexes.[44] Bulk magnetization measurements were obtained from a standard Quantum Design MPMS SQUID magnetometer. The samples consisted of randomly oriented Mn(acac)$_3$ microcrystals with a total mass of 169.07 mg. A small plastic can (0.273 mL polyethylene vial, Scienceware from Bel-Art Products, Pequannock, NJ) and plastic straw were used as the sample holder during the measurements. Magnetization versus temperature measurements were run from 2 to 300 K. The sample was zero-field cooled (ZFC) to 2 K before a measuring field of 0.1 T (1000 G) was applied. Data were then recorded while warming the sample from the lowest temperature. The sample was then cooled again to 2 K, but in the presence of a 0.1 T field, and additional field-cooled (FC) data were acquired. Differences between FC and ZFC magnetization were within experimental error. Magnetization versus field measurements were performed at 2 and 5 K over the field range 0 to 7 T. The diamagnetic contribution of each sample was estimated from Pascal's constants:[46] $\chi_D = -109 \times 10^{-6}$ emu/mol.

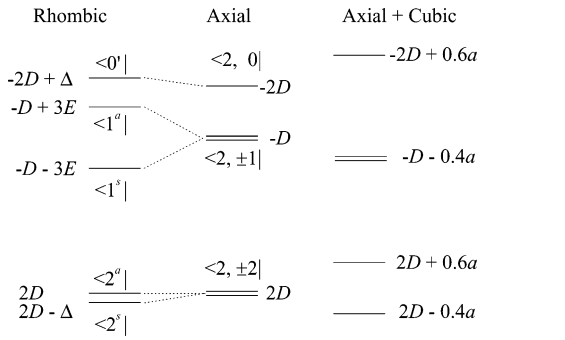

Figure 1. Energy diagram for an $S = 2$ system undergoing axial zero-field splitting (negative D) and with additional rhombic zero field splitting ($E \neq 0$) or with additional cubic zero-field splitting ($a \neq 0$). In the rhombic case, an EPR transition (often referred to as the "non-Kramers transition") between the states labeled $\langle 2^a|$ and $\langle 2^s|$ is partially allowed and observable at low applied magnetic field. Its intensity is enhanced by use of parallel mode detection.[33,54]

Theory for EPR Spectra and Magnetic Data. To analyze the EPR spectra and magnetic data, we applied the standard spin Hamiltonian for an $S \geq 2$ spin state with axial distortion about a tetragonal axis[2] and a small rhombic distortion (only to second order):

$$\mathscr{H} = \beta B \cdot \mathbf{g} \cdot S + B_4(O_4^0 + 5O_4^4) + B_2^0 O_2^0 + B_2^2 O_2^2 + B_4^0 O_4^0 \quad (1a)$$

Equation 1a can be rewritten with commonly used zfs parameters as

$$\mathscr{H} = \beta B \cdot \mathbf{g} \cdot S + (a/6)[S_x^4 + S_y^4 + S_z^4 - (1/5)S(S+1)(3S^2 + 3S - 1)] + D(S_z^2 - S(S+1)/3) + E(S_x^2 - S_y^2) + (F/180)[35S_z^4 - 30S(S+1)S_z^2 + 25S_z^2 - 6S(S+1) + 3S^2(S+1)] \quad (1b)$$

so that $D \equiv 3B_2^0$, $E \equiv B_2^2$, $F \equiv 180B_4^0$, and $a \equiv 120B_4$. The zero-field energy levels resulting from this spin Hamiltonian for $S = 2$ are shown in Figure 1. It was not possible to extract fourth-order zfs parameters (a, F) from HFEPR spectra; however, X-band results suggest a cubic zfs term, a, on the order of 0.15(5) cm^{-1}. The ligand-field analysis (Supporting Information) also provides an additional estimate of a. A spin Hamiltonian for $S = 2$ can also include higher order field-dependent (Zeeman) terms, such as BS^3,[47] which can complicate determination of g values; however, such terms were not considered here.

(44) Krzystek, J.; Park, J.-H.; Meisel, M. W.; Hitchman, M. A.; Stratemeier, H.; Brunel, L.-C.; Telser, J. *Inorg. Chem.* **2002**, *41*, 4478−4487.
(45) Hassan, A. K.; Pardi, L. A.; Krzystek, J.; Sienkiewicz, A.; Goy, P.; Rohrer, M.; Brunel, L.-C. *J. Magn. Reson.* **2000**, *142*, 300−312.
(46) O'Connor, C. J. *Prog. Inorg. Chem.* **1982**, *29*, 203−283.
(47) McGavin, D. G.; Tennant, W. C.; Weil, J. A. *J. Magn. Reson.* **1990**, *87*, 92−109.

Computer Simulation of EPR Spectra and Magnetic Data. Two different programs were used to extract numerical values of spin Hamiltonian parameters from the experimental EPR spectra. A locally written program calculates the EPR transition energies and probabilities from the eigenvalues and eigenvectors, respectively, obtained by diagonalization of the spin Hamiltonian matrix, with B_0 along a canonical (x, y, or z) axis. These were used to create characteristic canonical resonance field vs EPR operating frequency dependencies. A program written by Weihe[48,49] was used to generate powder pattern EPR spectra for particular frequencies, allowing direct assignment of the observed EPR transitions. The program is also based on a full-matrix diagonalization procedure and is therefore adequate to spin systems with any value of zfs parameters relative to the operating frequency. Our use of the program assumed collinearity of the **g** and **D** matrixes, as is usually done for high-symmetry molecules,[36] such as $Mn(acac)_3$, although in low-symmetry molecules this assumption may not be valid[14] and the program allows for noncollinearity. The program also takes into account the Boltzmann population factor in calculating the transition intensities. X-band spectra, which included resolved hyperfine splitting, were fit using the XSophe simulation/fitting program (version 1.0) obtained from Bruker, Inc.

Magnetic susceptibility and field-dependent magnetization data were fit using locally written programs employing the same spin Hamiltonian (eq 1b, with only second-order terms) as for the EPR data. Exact solutions to the spin Hamiltonian (matrix diagonalization using the EISPACK routines) for either axial or rhombic systems were fit to the data (using the program DSTEPIT from QCPE, Bloomington, IN). Because magnetic data are relatively insensitive to the sign of D, fits were performed with D constrained to have either negative or positive values, with E given the same sign, where applicable, and constrained to $|E/D| \leq 1/3$. All software for analysis of EPR and magnetic data are available as FORTRAN source code from the corresponding author.

Computer Analysis of Ligand-Field Parameters. Ligand-field analysis was performed using both a locally written program that calculates energy levels and EPR or electronic transitions using only the quintet (^{5}D) basis set, and the program LIGFIELD, written by J. Bendix.[50] LIGFIELD is an extremely versatile and powerful program that can use any d orbital basis set in ligand-field calculations and parametrizes the d orbital energies using either a crystal-field[51] or angular overlap model (AOM)[52] approach. Calculations here using LIGFIELD employed the entire basis set (210 microstates) for d^4.

Results

HFEPR of Frozen Solution $Mn(acac)_3$. Our solvent of choice for HFEPR was dichloromethane/toluene (3:2 v/v), which is a glassing solvent system employed in conventional EPR and one in which $Mn(acac)_3$ is quite soluble (100 mM). The resulting HFEPR spectra at 20 K and three different frequencies are shown in Figure 2. At lower frequencies (ν < ca. 250 GHz) the spectra are dominated by a single peak at low field (1.2 T at 193 GHz; Figure 2A) and a doublet at somewhat higher fields (4.8 and 5.5 T at 193 GHz; Figure 2A). There are also several weaker features in the spectra. With increasing frequency, the single peak moves to higher fields and loses intensity, so that it is not detectable above 350 GHz. The two lines in the doublet also move to higher fields and approach each other (Figure 2C), eventually to merge into a single line at the frequency of 386 GHz (Figure 2E). At higher frequencies (above 250 GHz) two very broad signals gradually appear (0.7 and 2.3 T, Figure 2C) that move to *lower* fields with increasing frequency. At 386 GHz one of them appears at almost exactly zero field (Figure 2E). There is also a strong signal at any given frequency (not shown) that appears at a field position corresponding exactly to $g = 2.00$, which does not belong to the $S = 2$ manifold, but originates from a high-symmetry Mn(II) ($S = 5/2$) impurity. No hfc from ^{55}Mn (100%, $I = 5/2$) is resolved in the frozen solution HFEPR spectra at any frequency or field.

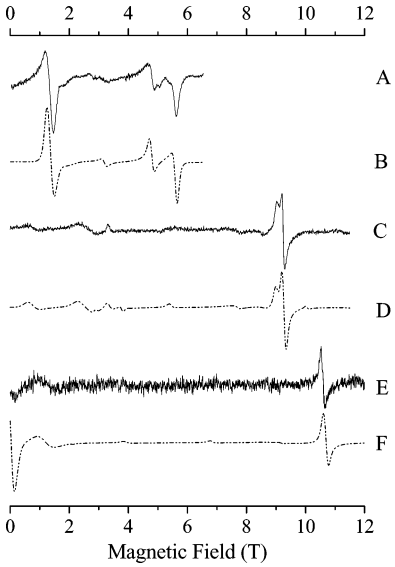

Figure 2. Experimental HFEPR spectra (solid lines) and simulations (dotted lines) of $Mn(acac)_3$ complex in CH_2Cl_2:toluene glass (3:2 v/v) at three different frequencies: (A, B) 192.83 GHz; (C, D) 338.61 GHz; (E, F) 385.66 GHz. Parameters: temperature, 20 K; magnetic field sweep rate, 0.5 T/min; field modulation, 8 kHz frequency, 1.5 mT amplitude; time constant, 0.3 s; millimeter or submillimeter power strongly dependent on frequency. Parameters used for simulations were the following: (B) $D = -4.50$ cm^{-1}, $|E| = 0.23$ cm^{-1}, $g_{iso} = 1.99$, single-crystal line width 60 mT (x and y transitions) and 150 mT (z transitions); (D) $D = -4.54$ cm^{-1}, $|E| = 0.27$ cm^{-1}, $g_{iso} = 1.99$, single-crystal line width 60 mT (x and y transitions) and 150 mT (z transitions); (F) $D = -4.54$ cm^{-1}, $|E| = 0.27$ cm^{-1}, $g_{iso} = 1.99$, single-crystal line width 60 mT (x and y transitions) and 250 mT (z transitions).

To interpret the spectra and extract spin Hamiltonian parameters from them, we use the quintet spin level diagram shown in Figure 1. Spectra collected at 386 GHz (Figure 2E) show a transition at, or very near, zero field. Taking account both the magnetic susceptibility results (see below) and the previous HFEPR data on the closely related complex, $Mn(dbm)_3$,[9] we concluded that the most likely assignment of the zero-field line is either the $|2, 2^a\rangle \rightarrow |2, 1^s\rangle$ or $|2, 2^s\rangle \rightarrow |2, 1^s\rangle$ transition. The energies of the corresponding ground-state levels are $2D$ or $[2D - \Delta]$, respectively, and that for the excited state is $[-D - 3E]$, where $\Delta =$

(48) Jacobsen, C. J. H.; Pedersen, E.; Villadsen, J.; Weihe, H. *Inorg. Chem.* **1993**, *32*, 1216−1221.
(49) Simulation software is available from Dr. H. Weihe; for more information see the www page: http://sophus.kiku.dk/software/EPR/EPR.html.
(50) Bendix, J.; Brorson, M.; Schäffer, C. E. *Inorg. Chem.* **1993**, *32*, 2838−2849.
(51) Ballhausen, C. J. In *Introduction to Ligand Field Theory*; McGraw-Hill: New York, 1962; pp 99−103.
(52) Schäffer, C. E. *Struct. Bonding* **1968**, *5*, 68−95.

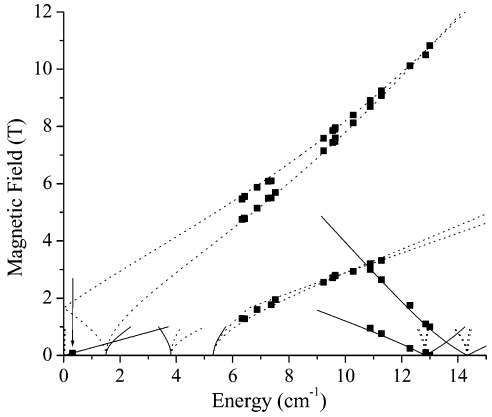

Figure 3. Plot of resonance field vs energy transition for a quintet ($S = 2$) spin state characterized by a rhombic zfs tensor along the three principal zfs axes. The squares are experimental data for $Mn(acac)_3$ while the curves were generated using the following spin Hamiltonian parameters: $|D| = 4.52$ cm^{-1}; $|E| = 0.25$ cm^{-1}; $g_{iso} = 1.99$. For clarity, transition branches that do not appear in experiment or appear at low intensities were arbitrarily cut off above 1 T. The solid lines represent simulated transitions along the *z* axis of the zfs tensor, while the dotted lines represent transitions along the *x* and *y* axes. The spectral features in Figures 2, 4, and 5 can be followed by drawing a line along the field axis at the given transition energy. The single, parallel transition observed in the X-band experiment (Figure 5) is highlighted by a vertical arrow at this energy (9.4 GHz, 0.31 cm^{-1}).

$3E^2/D$, ignoring the fourth-order Hamiltonian terms. The two transitions thus would appear at $3|D + E|$ and $|3(D + E) + \Delta|$. For an expected small value of Δ, and considering the large line widths, these two transitions can be treated as degenerate. This immediately yields an approximate value of $|D + E|$ equal to 4.27 cm^{-1}. This constraint on D and E obtained from zero-field resonance was subsequently used in spectral simulations, as presented in Figure 2 below the corresponding experimental spectra. The optimal parameters at lower frequencies (190−220 GHz) were $|D| = 4.50$ and $|E| = 0.23$ cm^{-1}, while at higher frequencies (290−390 GHz) a better agreement was found with $|D| = 4.54$ and $|E| = 0.27$ cm^{-1}. In each case the g factor was found to be practically isotropic and equal to 1.99. To derive frequency-independent spin Hamiltonian parameters, we plotted the resonance field vs operating frequency (see Figure 3), and best-fitting all of the experimental points led to the following spin Hamiltonian parameters: $|D| = 4.52$; $|E| = 0.25$ cm^{-1}; $g_{iso} = 1.99$. To determine the sign of D we performed a series of low-temperature experiments. Such an experiment, at 218 GHz and 4.5 K, is shown in Figure 4, together with two simulated spectra: one calculated using a negative value of $D = -4.50$ cm^{-1}; the other a positive value of the same magnitude. It is evident that a much better agreement between the experiment and simulation is obtained for the case of negative D. The final values of spin Hamiltonian parameters of $Mn(acac)_3$, including experimental errors, which we estimate as ± 0.02 cm^{-1} for D and E and 0.01 for the g factor, are given in Table 1, together with those for related complexes.[53] As is outlined below, the second-order zfs terms D and E may contain unresolved fourth-order zfs terms, F and particularly a.

(53) Since the only parallel transitions were recorded at very low fields, the accuracy of determining g_z is possibly lower than that obtained for $g_{x,y}$.

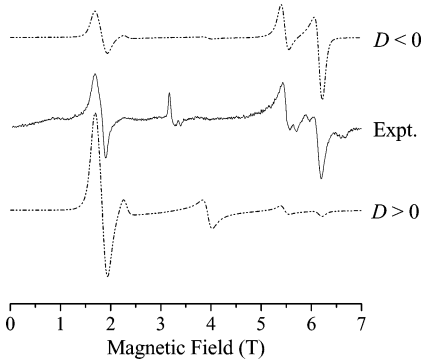

Figure 4. Determining the sign of D: low-temperature experimental HFEPR spectrum of $Mn(acac)_3$ complex in CH_2Cl_2:toluene glass (solid line, center) and simulations using the values $D = -4.50$ cm^{-1} (top) and $+4.50$ cm^{-1} (bottom), each with $|E| = 0.23$ cm^{-1}. Parameters: temperature, 4.5 K; frequency, 217.81 GHz; other experimental and simulation parameters as in Figure 2. The sharp features in the experimental spectrum at ca. 3.2 and 5.7 T originate from solid oxygen in the sample area.

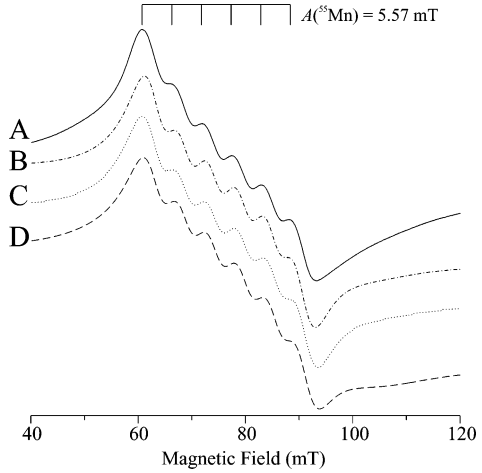

Figure 5. (A) X-band EPR spectrum of $Mn(acac)_3$ as a 10 mM solution in CH_2Cl_2:toluene (3:2 v/v) at 9.42 GHz recorded in parallel mode polarization at 5 K. Instrumental settings as follows: microwave power, 1 mW; field modulation, 100 kHz frequency, 0.8 mT amplitude; time constant, 20 ms; average of 6 spectra; (B) simulation using $g_{iso} = 2.17$, $D = -4.52$ cm^{-1}, $|E| = 0.25$ cm^{-1}; (C) simulation using $g_{iso} = 2.00$, $D = -4.52$ cm^{-1}, $|E| = 0.44$ cm^{-1}; (D) simulation using $g_{iso} = 2.00$, $D = -4.52$ cm^{-1}, $|E| = 0.25$ cm^{-1}; $|a| = 0.17$ cm^{-1}. In all simulations, the hfc constant $A(^{55}Mn)_{iso}$ was set to 5.57 mT (156 MHz).

Powder patterns, as observed in the frozen solution of $Mn(acac)_3$, do not allow, however, one unequivocally to determine these terms, and single-crystal studies are usually necessary to achieve that purpose.[16,36]

X-Band EPR of Frozen Solution $Mn(acac)_3$. The X-band (9.41 GHz) EPR spectrum using parallel polarization recorded for $Mn(acac)_3$ in CH_2Cl_2/toluene (3:2 v/v) at 5 K is shown in Figure 5A. As has been similarly observed in other Mn(III) complexes,[28,31−34] a single line, centered at ∼74 mT, is found. This signal results from an EPR transition between the two spin levels originating from the $\langle 2, 2^s|$ and $\langle 2, 2^a|$ zero-field states (see Figure 1), which is enhanced using parallel mode detection.[33,54] In sharp contrast to the HFEPR spectra, a sextet due to partly resolved hfc from ^{55}Mn is clearly visible. Resolved hfc has been observed in several other such cases[28,31,32] and is particularly useful in determin-

(54) Hendrich, M.; Debrunner, P. *Biophys. J.* **1989**, *56*, 489−506.

Table 1. Electronic Parameters from Resonance Spectroscopic Techniques for Mn^{3+} with Pseudooctahedral Coordination and Oxygen/Nitrogen Donor Ligands

complex	g_x, g_y, g_z	D, $\|E\|$ (cm^{-1})	A_x, A_y, A_z (^{55}Mn) (MHz)
$Mn(acac)_3$[a]			
expt	1.99(1) (isotropic)	−4.52(2), 0.25(2)	156(2) (isotropic)
axial calcd	1.99, 1.99, 1.96	−4.51	
rhombic calcd	1.99, 1.99, 1.96	−4.49, 0.27	
$Mn(dbm)_3$[b]			
expt	1.99, 1.99, 1.97	−4.35, 0.26	
axial calcd	1.99, 1.99, 1.96	−4.57	
rhombic calcd	1.99, 1.99, 1.96	−4.55, 0.28	
$Mn^{3+}[TiO_2]$[c]	2.00, 2.00, 1.99	−3.4, 0.116[c]	253, 242, 158
$[Mn(OD_2)_6]^{3+}$[d]		−4.524, 0.276	
$[Mn(terpy)(N_3)_3]$[e]	2.00, 1.98, 2.01	−3.29, 0.51	
[Mn(salen)(NMO)][f]	2.0, 2.0, 1.98	−2.50, 0.269	190, 190, 125

[a] This work; Hacac is 2,4-pentanedione. Experimental values for D, $|E|$ are from HFEPR on frozen solution complex (in CH_2Cl_2:toluene glass, 3:2 v/v). HFEPR on immobilized powder complex gave the following: $D = -4.60(5)$ cm^{-1}; $|E| = 0.30(5)$ cm^{-1}; $g = 1.99(2)$ (isotropic). Consensus fit values from magnetic measurements on powder complex are the following: $D = -4.5(3)$ cm^{-1}; $g_{x,y} = 2.00(5)$; $g_z = 1.85(10)$; $|E|$ not determined. Hyperfine coupling is from X-band parallel mode EPR in frozen solution, which also suggested cubic zfs, $a = 0.15(5)$ cm^{-1}. Powder magnetic susceptibility studies by Gregson et al. gave $D = +3.1$ cm^{-1}.[43] For the axial case, the calculated D values used the following parameters (all in cm^{-1}): $e_\sigma^{x,y} = 8755$; $e_\pi^{x,y} = 2090$; $e_\sigma^{z} = 3995$; $e_\pi^{z} = 290$; with Racah parameters[70] $B = 1140$, $C = 3650$; with $\zeta = 348$. (Calculation using Racah parameters[69] $B = 950$ and $C = 4085$, with $\zeta = 355$, yields $D = -4.24$ cm^{-1}.) These calculations suggested cubic zfs, $a \approx 0.1$ cm^{-1}. For the rhombic case, the calculated D and E values used the following parameters (all in cm^{-1}): $e_\sigma^{x} = 8955$; $e_\pi^{x} = 2290$; $e_\sigma^{y} = 8555$; $e_\pi^{y} = 1890$; with all other parameters as in the axial calculation. The calculation of g values uses only a first-order perturbation theory expression,[2] which we have used previously.[3] [b] HFEPR study by Barra et al. on powder complex; Hdbm is 1,3-diphenyl-1,3-propanedione.[9] The calculated D value used the following parameters (all in cm^{-1}) for the axial case: $e_\sigma^{x,y} = 9333$; $e_\pi^{x,y} = 2500$; $e_\sigma^{z} = 4833$; $e_\pi^{z} = 1000$; $B = 1140$; $C = 3675$; $\zeta = 360$. Data for the rhombic case: $e_\sigma^{x} = 9595$; $e_\pi^{x} = 2570$; $e_\sigma^{y} = 9080$ cm^{-1}; $e_\pi^{y} = 2430$; all other parameters as in the axial calculation. [c] EPR study by Gerritsen and Sabisky on single-crystal Mn^{3+} doped into rutile.[36] A cubic zfs term was also determined: $a = 0.13$ cm^{-1}. [d] Inelastic neutron scattering (INS) study by Basler et al. on powder $CsMn(SO_4)_2 \cdot 12D_2O$.[35] This study directly measured the fine structure transitions at zero field; hence, no g values (nor hyperfine coupling) were determined. [e] HFEPR study by Limburg et al. on powder complex;[14] terpy is 2,2′:6′,2″-terpyridine, so that the complex has an N_6 donor set, as opposed to O_6 in all of the other cases. [f] Parallel mode X-band EPR study by Campbell et al.[28] on frozen CH_2Cl_2 solution; salen is *N*,*N*′-ethylenebis(salicylideneaminato) dianion, and NMO is *N*-methylmorpholine *N*-oxide.

ing the number of magnetically inequivalent Mn sites of interest. In this case, only one Mn(III) site is evident, as expected. The ^{55}Mn hfc constant observed for $Mn(acac)_3$ is 5.57 mT (156 MHz, 52×10^{-4} cm^{-1}), which is quite similar to other values reported for Mn^{3+}, as given in Table 1. As the temperature is increased, resolution of hfc becomes poorer and is lost upon reaching ∼30 K. The signal is broadened beyond observation at temperatures above 45 K.

For simulation of the observed X-band spectrum, we began by use of the zfs parameters determined from HFEPR. These produced a simulated line that was shifted to higher field by ca. 7 mT relative to the observation. To bring the simulated line into agreement with the experiment, the XSophe fitting routine simply increased the g value, optimizing at $g = 2.17$ (Figure 5B). Although the agreement is excellent, it is obvious that such a high g value does not represent a physically meaningful parameter for Mn(III), g being an "effective g" in this case. With constrainment of g to 2.00 and D to -4.52 cm^{-1} (the HFEPR and magnetic study value), agreement was reached only by significantly increasing $|E/D|$ to 0.098 (Figure 5C), which gives $|E| = 0.44$ cm^{-1}, a magnitude unsuitable to interpret the HFEPR data. To solve this dilemma, we referred to the work of Gerritsen and Sabisky,[36] who observed that the energy difference between the levels $|2^a\rangle$ and $|2^s\rangle$ depends not only on the factor $\Delta = 3E^2/D$, and thus on the rhombicity ratio $|E/D|$, but also on the cubic zfs term a (see eq 1). Since the energy gap between the $|2^a\rangle$ and $|2^s\rangle$ levels determines the position of the non-Kramers X-band signal, it is necessary in such a case to include fourth-order spin Hamiltonian terms in the simulation. The result is shown in Figure 5D. One can see that a very good agreement with experiment is reached by keeping the HFEPR zfs values unchanged but introducing $a = 0.17$ cm^{-1}.[55] Since equally good agreement obtains when using quite different spin Hamiltonian parameters in the simulations, as seen in Figure 5, it follows that the X-band non-Kramers signal alone does not unequivocally allow determination of all of these parameters. It follows also that the zfs parameters obtained from HFEPR do indeed contain the unresolved cubic zfs term a, on the order of 0.15(5) cm^{-1}. Further simulations of HFEPR spectra convinced us, however, that the effect of a cubic term a of this magnitude is far smaller at high frequencies, amounting to ∼0.1% shift of the resonance field at 285 GHz, than at X-band, where the same effect is responsible for a 10% shift of the resonance line.

It should also be mentioned that the observed X-band signal of $Mn(acac)_3$ in toluene/CH_2Cl_2 has a rather unusual shape. Since it corresponds to a z turning point of the respective powder pattern (see Figure 3), it should be absorptive in shape, as indeed observed in the Mn(salen)/NMO complex.[28] Instead, the signal is derivative in shape. An essentially identically shaped X-band parallel polarization signal was reported (without simulations) by Dexheimer et al. for $Mn(acac)_3$ in butyronitrile/ propionitrile frozen solution at 12 K,[34] so that this unusual line shape appears to be a characteristic of this complex. In the simulations, we reproduced this line shape by attributing very large line widths to the respective x and y turning points of the same transition, which, however, does not explain the phenomenon itself.

HFEPR of Solid-State $Mn(acac)_3$. HFEPR experiments on loose, polycrystalline $Mn(acac)_3$ proved inconclusive. The sample undergoes partial torquing in the magnetic field that causes several irreproducible peculiarities to appear in the spectra, which are indistinguishable from real turning points of the powder pattern. It was thus impossible to interpret the spectra reliably. Constraining the crystallites in a KBr pellet did improve the spectra, although some artifacts remained that could not be reproduced in simulations, pointing at still imperfect randomization (see Figure S1, Supporting Information). The importance of the obtained

(55) XSophe uses a spin Hamiltonian form different from eq 1, employing constants b_{04} and b_{44}, defined as $B_4^0/60$, and $B_4^4/60$, respectively. To convert these to a, we observed that $B_4 = a/120$, as in eq 1, is equal to B_4^0 and $5B_4^4$. We thus obtain $a = 2b_{04} = 2b_{44}/5$.

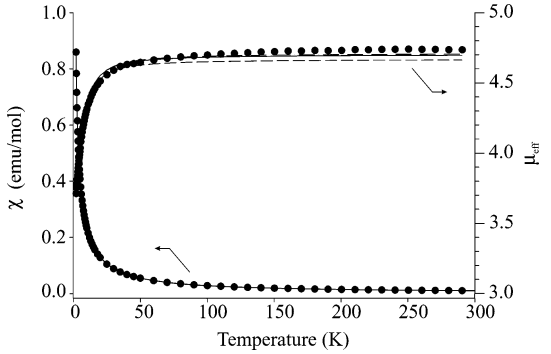

Figure 6. Magnetic data for $Mn(acac)_3$, presented both as molar paramagnetic susceptibility (χ, emu/mol) versus temperature (left vertical axis) and as effective magnetic moment (μ_{eff}) versus temperature (right vertical axis). Best fit lines are also shown as follows: solid line, $D \equiv -4.60$, $E \equiv -0.30$ cm^{-1}, $g_{x,y} \equiv 1.99$, $g_z = 1.76$ (values for D, E, and $g_{x,y}$ are from HFEPR of solid complex); dot−dashed line, $D = -4.70$, $E \equiv 0$ cm^{-1}, $g_{x,y} \equiv 1.99$, $g_z = 1.76$ (value for $g_{x,y}$ is from HFEPR of solid complex); dashed line, $D = -4.54$, $E \equiv 0$ cm^{-1}, $g_{x,y} = 1.98$, $g_z = 1.76$. Note that, in the plot of χ vs T, the fit lines are indistinguishable and are only barely so in the plot of μ_{eff} vs T. Fits using $D > 0$ (not shown) are much less successful. All fits using rhombic zfs (i.e., allowing $E \neq 0$) yielded either no improvement over axial fits or yielded less meaningful parameters, regardless of constraints on the symmetry of the **g** matrix.

pellet spectra is that they demonstrate that the spin Hamiltonian parameters of the polycrystalline solid do *not* differ significantly from those obtained from the frozen solution (see Table 1).

Magnetic Measurements and Analysis of $Mn(acac)_3$. The finding that $Mn(acac)_3$ in frozen solution exhibited a negative value for D, indicating tetragonal elongation, combined with the correspondence between solid-state and frozen-solution HFEPR prompted us to reexamine the solid-state magnetic properties of this complex. Temperature-dependent magnetic susceptibility measurements over the temperature range 2−300 K at 0.1 T were performed and are presented in Figure 6. Field-dependent magnetization measurements at both 2 and 5 K over the range 0−7 T were also made, and the results are shown in Figure S2.

The magnetic data were fitted primarily by use of an axial zfs tensor. As is often, although not always the case,[56] for powder magnetic measurements, use of a rhombic zfs tensor did not always improve the fits and/or yield meaningful parameters. However, constraining the axial fits so that either $D > 0$ or $D < 0$ was extremely informative, providing an overall consistent picture of $Mn(acac)_3$ in our study. Fits using $D > 0$ were unsuccessful at fitting either the susceptibility or magnetization data, while fits using $D < 0$ gave this parameter in excellent agreement with that obtained from HFEPR: $D = -4.5 \pm 0.3$ cm^{-1} as a consensus value derived from all of the magnetic measurements. Furthermore, fits of the magnetic data with the rhombic zfs parameters fixed at the values obtained for powder $Mn(acac)_3$ from HFEPR were equally successful (see Figures 6 and S2). Specific fit values are given in the captions to Figures 6 and S2. Little deviation from $g_{x,y}$ ($g_\perp$) = 2.00 was required for fitting; however, the susceptibility fits suggested g_z ($g_\parallel$) ≈ 1.8 ± 0.1. First-order perturbation theory indicates that $2.00 \gtrsim g_{x,y} > g_z$,[2,36] as is generally seen experimentally (Table 1), although this low g_z value is peculiar and may incorporate other factors not included in the spin Hamiltonian, such as intermolecular magnetic exchange forces or excited-state mixing.[46] The magnetization fits, however, suggested $g_z \approx 1.9 \pm 0.1$ with the consequence that there is no obvious anomaly nor much information associated with the g values for $Mn(acac)_3$.

The finding that our magnetic measurements on $Mn(acac)_3$ supported a value for $D = -4.5(3)$ cm^{-1} prompted us to return to the data reported by Gregson et al., who found $D = +3.1(1)$ cm^{-1},[43] in case there was some discrepancy in data analysis between the two studies. Digitization of their Figure 4 allowed us to fit their data using our methods, which clearly confirmed that the parameters they reported were quite appropriate, while those we found for ostensibly the same compound were wholly unsuccessful.

Optical Studies of Frozen $Mn(acac)_3$ Solution. To ensure correspondence between EPR results obtained here in dichloromethane/toluene and previous electronic absorption studies using cyclohexane solutions,[37,38,57] we recorded visible-NIR spectra on $Mn(acac)_3$ in both solvent systems. Visible (1 mM) and NIR (10 mM) spectra in the two solvent systems were identical within experimental error (see Figure S3, Supporting Information) and in agreement with previously reported spectra.[37,38]

Discussion

The most succinct result obtained from the EPR is (a) the negative sign of the zfs parameter D and (b) the magnitude of $|D|$ equal to 4.52 cm^{-1} in frozen solution and ∼4.6 cm^{-1} in the solid state. The negative sign of D is in agreement with all of the other Mn(III) (and Cr(II)) systems studied by HFEPR.[58] Our solid-state magnetic measurements on $Mn(acac)_3$ likewise support a negative value for D. Although magnetic susceptibility fits can be rather insensitive to the sign of D,[40] this does not appear to be the case here, either for our data or for the data of Gregson et al.,[43] who reported a positive D.

The magnitude of D obtained by Gregson et al. also differs significantly from that found here: 3.1(1) cm^{-1} versus 4.5−4.6 cm^{-1} (this range comprises both our solid-state *and* frozen-solution data; no determination of E is possible from either their or our powder magnetic susceptibility data). Table 1 lists the zfs parameters that have been accurately determined for pseudooctahedral Mn(III) complexes with O/N donors. It can be seen that the difference between these two forms of $Mn(acac)_3$ is greater than what can be found for

(56) Orendác, M.; Čizmár, E.; Orendácová, A.; Černák, J.; Feher, A.; Meisel, M. W.; Abboud, K. A.; Zvyagin, S.; Sieling, M.; Rieth, T.; Lüthi, B. *Phys. Rev. B* **2000**, *61*, 3223−3226.

(57) $Mn(acac)_3$ is sufficiently soluble in cyclohexane for UV−vis−NIR but not so for HFEPR.

(58) A significant exception is the complex $[Mn(cyclam)_2I_2]I$, which has very recently been studied by HFEPR and exhibits $D = +0.60$ cm^{-1}.[15] However, this positive D value is due to LMCT interactions involving the relatively low-energy iodo ligands, which themselves have very large spin−orbit coupling interactions, with the result that a simple ligand-field description using only $3d^4$ states is inappropriate for Mn(III) in this complex. No such complication holds for Mn(III) with oxygen donor ligands, as is the case here.

chemically distinct species: A value of $D = -3.4$ cm^{-1} was determined by single-crystal EPR for Mn^{3+} with six oxo ligands (rutile lattice),[36] and a HFEPR study gave $D = -3.29$ cm^{-1} (with a large E term) for a Mn(III) complex with six nitrogen donor ligands.[14] Particularly reassuring is the fact that the zfs parameters determined here for the frozen solution and solid $Mn(acac)_3$ are very close to those reported by Barra et al. ($D = -4.35$; $|E| = 0.26$ cm^{-1})[9] in their HFEPR study of $Mn(dbm)_3$, which also included a crystal structure that indicated axial elongation.

The most plausible explanation for the difference between our results and those of Gregson et al. lies in the multiple crystal structures of $Mn(acac)_3$. Remarkably, the crystal structure first reported for $Mn(acac)_3$ showed no Jahn−Teller distortion;[59] however, it was subsequently proposed by Fackler and Avdeef that the original structure was likely that of $Co(acac)_3$, and authentic $Mn(acac)_3$ indeed exhibits a tetragonally distorted geometry.[60] This monoclinic form of $Mn(acac)_3$ is known as β-$Mn(acac)_3$[61] and exhibits very little trigonal distortion from a regular octahedron.[60] There is a distinct tetragonal compression, with axial Mn−O bond lengths of 1.95 Å and equatorial Mn−O bonds lengths of 2.00 Å.[60,62] Subsequently, Stults et al. reported the crystal structure of second monoclinic form, known as γ-$Mn(acac)_3$.[63] In this structure, the geometry about Mn^{3+} is very close to D_{4h} symmetry, with a distinct tetragonal elongation: The two axial Mn−O bond lengths are 2.111 Å, and the four equatorial Mn−O bond lengths are 1.945 Å.[64]

Fackler and Avdeef used the crystallographic information combined with vibrational data to calculate the Jahn−Teller distortion using a crystal-field model. Both tetragonal compression and elongation were predicted, with the resulting bond lengths in reasonable agreement with those found experimentally for β- and γ-$Mn(acac)_3$, respectively.[60,65] However, the origin of compression versus elongation in the two crystal forms was not clear, and Fackler and Avdeef suggested that lattice forces could be more responsible for this difference, rather than intramolecular electronic effects.[60] A consequence of this difference, however, is that it is of interest to determine the structure of $Mn(acac)_3$ in solution, where lattice forces should be absent.

In view of the above, it is plausible that the compound Gregson et al. synthesized and investigated by magnetic methods was composed largely of β-$Mn(acac)_3$ for which the compressed structure[60] would lead to $D > 0$, while the commercial material studied here was composed largely of γ-$Mn(acac)_3$,[63] for which the elongated structure would yield $D < 0$. Frozen-solution studies clearly indicate that the isolated $Mn(acac)_3$ complex exhibits tetragonal elongation, as is the case for other, related Mn(III) systems.

A final aspect of the Jahn−Teller distortion in $Mn(acac)_3$ is whether this process is dynamic and that the two crystal structures result from trapping the complex in different potential energy wells of a multiple-well ("Mexican hat")[66] potential energy surface. Simple complexes with $S = 1/2$ electronic ground states and homoleptic, unidentate ligands, such as $[Ni(CN)_6]^{3-}$ (low-spin $3d^7$)[67] and $[Cu(H_2O)_6]^{2+}$ ($3d^9$)[68] exhibit very interesting temperature-dependent EPR behavior due to this phenomenon. At lower temperatures (~50 K), an anisotropic EPR signal typical for, e.g., tetragonally distorted low-spin $3d^7$ ($d_{z^2}{}^1$) is observed, but as the temperature is increased (~240 K), an isotropic EPR spectrum results, due to dynamic averaging of this distortion.[67] Unfortunately, the EPR properties of $Mn(acac)_3$ make it unsuitable for observation of any hint of this phenomenon. EPR spectra for this non-Kramers system are observable only at low temperatures (<45 K), and in any case, it is likely that a complex with bidentate ligands would not allow dynamic averaging except at much higher temperatures than those needed for complexes with unidentate ligands.

Thanks to X-band parallel mode EPR, we can observe hfc for Mn(III) in this complex, which has so far not been possible using HFEPR, in our or other workers' studies of Mn(III) complexes.[9,14,15,39] The hfc is slightly smaller than that for Mn^{3+} in rutile (see Table 1), wherein a single-crystal study allowed determination of the complete ^{55}Mn hfc matrix. Both complexes have an O_6 donor set; however, there may be more extensive spin delocalization onto the π-conjugated acac ligands than in the oxide lattice of rutile, thus lowering the ^{55}Mn hfc in $Mn(acac)_3$.

Following the work of Barra et al.,[9] we can analyze quantitatively the parameters determined for $Mn(acac)_3$ in solution, making use of the reported electronic absorption data for the complex.[38] A diagram of the quintet electronic energy levels, roughly to scale, is shown in Figure 7. A detailed description of our analysis is given in the Supporting Information. The analysis made use of the program LIGFIELD, written by Bendix,[50] which uses the entire free-ion basis set for d^4 and allows either crystal-field or angular overlap model (AOM)[52] parametrization to be used.

As described in the Supporting Information, it is possible to match exactly the observed axial and rhombic zfs by use of reasonable crystal-field and free-ion (Racah, spin−orbit coupling)[69,70] parameters. The study by Barra et al. on the related complex, $Mn(dbm)_3$,[9] included a detailed analysis of the electronic parameters using the AOM, which has been

(59) Morosin, B.; Brathovde, J. R. *Acta Crystallogr.* **1964**, *17*, 705−711.
(60) Fackler, J. P., Jr.; Avdeef, A. *Inorg. Chem.* **1974**, *13*, 1864−1875.
(61) There is also an orthorhombic form of $Mn(acac)_3$, known as α-$Mn(acac)_3$, but no bond distances nor angles have been reported.
(62) The individual Mn−O bond lengths are 1.931, 1.956, 1.984, 1.991, 2.003, and 2.020 Å.
(63) Stults, B. R.; Marianelli, R. S.; Day, V. W. *Inorg. Chem.* **1979**, *18*, 1853−1858.
(64) The individual Mn−O bond lengths are 2.112, 2.109, 1.942, 1.934, 1.933, and 1.931 Å.
(65) Using an undistorted Mn−O bond length of 1.985 Å, the tetragonally compressed (β) complex was predicted to have axial and equatorial bond lengths of 1.893 and 1.998 Å, respectively, and the tetragonally elongated (γ) complex to have to have axial and equatorial bond lengths of 2.026 and 1.932 Å, respectively.
(66) Hathaway, B. J. *Struct. Bonding (Berlin)* **1984**, *57*, 1−60.
(67) Wang, Y. L.; Beach, M. W.; Pappenhagen, T. L.; Margerum, D. W. *Inorg. Chem.* **1988**, *27*, 4474−4472.
(68) Riley, M. J.; Hitchman, M. A.; Mohammed, A. W. *J. Chem. Phys.* **1987**, *87*, 3766−3778.
(69) Figgis, B. N.; Hitchman, M. A. *Ligand Field Theory and its Applications*; Wiley-VCH: New York, 2000.
(70) Mabbs, F. E.; Collison, D. *Electron Paramagnetic Resonance of d Transition Metal Compounds*; Elsevier: Amsterdam, 1992.

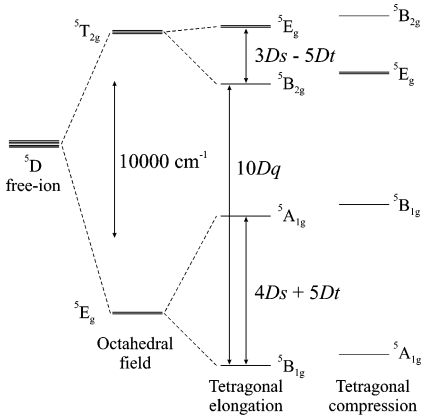

Figure 7. Electronic states of Mn^{3+} in D_{4h} symmetry. Only the spin quintet states are shown, and spin−orbit coupling effects are not included. The energy splittings are given using the crystal-field parameters as defined by Ballhausen.[51] The energy levels are roughly to scale and are based on the assignments by Davis et al. for $Mn(acac)_3$ (see text).[38] The case of tetragonal elongation for $Mn(acac)_3$ was proposed by Davis et al.[38] and is supported here by EPR data. The case of tetragonal compression was proposed by Gregson et al. on the basis of powder magnetic susceptibility studies.[43]

successfully used in other HFEPR studies as well.[8] By use of several simplifying assumptions (see Supporting Information), it is possible to derive AOM parameters that match quite well the observed zfs for $Mn(acac)_3$ (see Table 1 for experimental data and calculations using both axial and rhombic AOM parameters). An axial model yields the AOM bonding parameters for $Mn(acac)_3$ in solution of $e_\sigma^{x,y} = 8755$ cm^{-1}, $e_\pi^{x,y} = 2090$ cm^{-1}, $e_\sigma^{z} = 3995$ cm^{-1}, and $e_\pi^{z} = 290$ cm^{-1}, which are quite similar to those proposed earlier for $Mn(dbm)_3$ (see Table 1) by Barra et al.,[9] who used a slightly different set of simplifying assumptions. The AOM parameters for these Mn(III) diketonates are similar to those for related Cr(III) complexes.[69,71]

Conclusions

HFEPR allows observation of the fine structure transitions in the classical coordination complex, $Mn(acac)_3$, in both frozen solution and as a powder. These results show the applicability of HFEPR toward the study of high-spin non-Kramers first-row transition metal ion complexes, in this case, one of Mn^{3+} ($3d^4$, $S = 2$). However, in contrast to Mn^{3+} complexes with axial symmetry, $Mn(acac)_3$ is not "EPR-silent": X-band EPR using parallel mode polarization exhibits a characteristic "non-Kramers" signal with resolved ^{55}Mn hyperfine coupling, indicating a single species in solution with hfc values typical for Mn^{3+}. It is nevertheless difficult to extract the relevant electronic spin Hamiltonian parameters solely from this low-frequency EPR spectrum, while multifrequency, high-field EPR readily allows determination of these parameters: $D = -4.52(2)$; $|E| = 0.25(2)$ cm^{-1}; $g = 1.99(1)$ (isotropic). The axial zfs for $Mn(acac)_3$ in frozen solution (CH_2Cl_2/toluene, 3:2 v/v) differs only very slightly from that found by HFEPR and magnetic measurements for the solid-state material. The negative sign of D indicates tetragonal elongation in both solution and the solid state. Our value for D is quite different in both sign and magnitude from that found in a much earlier magnetic susceptibility study ($D = +3.1$ cm^{-1}).[43] Crystal structures of $Mn(acac)_3$ show this static Jahn−Teller distortion, as expected; however, structures with both elongation and compression are found.[60,63] Presumably, our solid-state study describes the elongated form (γ-$Mn(acac)_3$[63]), while the compressed form (β-$Mn(acac)_3$[60]) was the subject of the previous study.[43] Elongation is found for porphyrinic complexes[11−13] and is expected for these five-coordinate (square pyramidal) complexes. Tetragonal elongation, however, is also found for Mn^{3+} and Cr^{2+} complexes with homoleptic six-coordinate (pseudooctahedral) geometry,[3,9,36] as well as for similar heteroleptic complexes.[14,42] The results obtained here for $Mn(acac)_3$ in frozen solution, combined with those for other octahedral high-spin $3d^4$ ions, suggest that axial elongation could be considered the "natural" form of Jahn−Teller distortion for this electronic configuration, while the compressed form found in β-$Mn(acac)_3$ might be an unusual consequence of as yet undetermined crystal-packing effects. Ligand-field analysis of the results for $Mn(acac)_3$ shows a coordination environment similar to that in $Mn(dbm)_3$[9] and related Cr(III) complexes.[69,71]

Acknowledgment. We thank Drs. J. Bendix and H. Weihe, both from the Ørsted Insitute, Copenhagen, Denmark, for providing us with the LIGFIELD program and for the SIM spectral simulation software, respectively. Both are also acknowledged for very helpful discussions, as is Prof. Dale W. Margerum, Purdue University. Financial support of the NHMFL and Roosevelt University (J.T.) and of the ACS (PRF No. 36163-AC5 for J.-H.P. and M.W.M.) is acknowledged as well.

Supporting Information Available: A detailed textual description of the crystal/ligand-field analysis for $Mn(acac)_3$, Table S1 listing electronic energy levels calculated for $Mn(acac)_3$ with varying ligand fields, and three figures showing KBr pellet HFEPR spectra for powder $Mn(acac)_3$, field-dependent magnetization data for powder $Mn(acac)_3$, and visible-NIR spectra for fluid-solution $Mn(acac)_3$. This material is available free of charge via the Internet at http://pubs.acs.org.

IC020712L

(71) Lever, A. B. P. *Inorganic Electronic Spectroscopy*, 2nd ed.; Elsevier: Amsterdam, 1984.